



# On experimentally locating saddle-points on a potential energy surface from observed dynamics



Yawen Xu <sup>a</sup>, Lawrence N. Virgin <sup>a,\*</sup>, Shane D. Ross <sup>b</sup>

<sup>a</sup> Department of Mechanical Engineering and Materials Science, Duke University, Durham, NC 27708, USA

<sup>b</sup> Engineering Mechanics Program, Virginia Tech, Blacksburg, VA 24061, USA

## ARTICLE INFO

### Article history:

Received 12 September 2018

Received in revised form 15 March 2019

Accepted 2 May 2019

### Keywords:

Nonlinear dynamics

System identification

Saddle point

Potential energy

Experimental mechanics

## ABSTRACT

This paper details a new method to estimate the location of *unstable* equilibria, specifically saddle-points, based on transient trajectories from experiments. We describe a system in which saddle-points (not easily observed in a direct sense) influence the behavior of trajectories that pass 'close-by' them. This influence is used to construct a model and thus identify a more accurate estimate of the location using a number of refinements associated with linearization and regression. Both simulations and experiments were conducted to verify the method. The experiment consists of a small ball rolling on a relatively shallow curved surface under the influence of gravity: a potential energy surface in two dimensions. Tracking the motion of the ball with a digital camera provides data that compares closely with the output of numerical simulation. The experimental results suggest that this method can effectively locate the saddle equilibria in a system, and the robustness of the approach is assessed relative to the effect of noise, size of the local neighborhood, etc., in addition to providing information on the local dynamics. Given the relative simplicity of the experiment system used and a priori knowledge of the saddle-points, it is a useful testing environment for system identification in a nonlinear context.

© 2019 Elsevier Ltd. All rights reserved.

## 1. Introduction

Conservative dynamical systems are typically associated with an underlying potential energy, and one can easily imagine in a nonlinear context a trajectory meandering through phase space, encountering and passing-by multiple stable and unstable equilibria as it goes [1,2]. Given a little positive energy dissipation we would expect a trajectory to end up in a position of stable equilibrium (a potential energy minimum), but which final state persists depends crucially on the role played by unstable equilibria (saddles of varying degrees of instability and local maxima) as well as the initial conditions [3,4]. However, by their very nature, unstable equilibria are very difficult to directly observe in an experiment.

It is also quite natural to ask the question: under what circumstances might trajectories *escape* the local confines of a potential energy minimum. In nonlinear systems we must consider stability *in-the-large*, where perturbations are not necessarily small and co-existing equilibria come into play [5]. This situation is quite straightforward for a single-degree-of-freedom (DOF) system in which the location of an adjacent unstable equilibrium (potential energy hill-top) is easily identified, and a trajectory effectively has no choice but to transition over the hilltop if it is to escape. However, in multi-DOF systems, the exit of trajectories would likely be influenced by the location of the various other equilibria that

\* Corresponding author.

E-mail addresses: [yawen.xu@duke.edu](mailto:yawen.xu@duke.edu) (Y. Xu), [l.virgin@duke.edu](mailto:l.virgin@duke.edu) (L.N. Virgin), [sdross@vt.edu](mailto:sdross@vt.edu) (S.D. Ross).

might be present as it explores the phase space, and this presents considerable challenges especially in an experimental context [6].

In order to fix these ideas in a relatively simple dynamical system setting, it is compelling to develop the analogy of a small ball rolling along a single-valued curved surface under the influence of gravity, and defined by a trajectory that lives in this 2D configuration space  $(X, Y)$ : a potential energy *surface*. In a linear system we might simply have a potential energy function in the form of a paraboloid [1], with a single minimum. However, in a nonlinear system the potential energy surface would typically contain a variety of turning points, including the possibility of saddle-points, that is, equilibria characterized locally by positive and negative curvature [7,8]. Despite the presence of stable manifolds, they are still unstable, and by definition, would not be easily identified in experiments. However, they typically play a crucial organizing role in the global dynamics of a system [9–11], for example, in defining catchment regions for stable equilibria, and it is easy to envision that a trajectory might find it energetically-easier, (if we include kinetic energy) to escape by passing through a saddle-point (a kind of mountain pass) rather than going right over a hill-top before perhaps ending up at a remote stable equilibrium. A railroad between villages in adjacent valleys is built around a mountain rather than directly over its peak.

There are many examples of structural and particle or rigid body mechanical systems in which behavior can be described in terms of two generalized coordinates. The double pendulum is a good example, in which there is a single stable equilibrium (the hanging down configuration) and three unstable ones (involving various inverted states). In a dynamics context this leads to a 4D phase space (with two velocities  $(\dot{X}(t), \dot{Y}(t))$  in addition to the positions  $(X(t), Y(t))$ ) [3]. Another example is a relatively slender shallow arch subject to snap-through to an inverted configuration after a perturbation. Depending on the geometry, this snap-through is often achieved with an asymmetric component (in addition to a vertical deflection) and thus is often modeled as a simplified 2-DOF system [4,12], despite it being a continuous elastic system. Here, we appeal to the ball-on-a-surface concept, used, for example, to successfully demonstrate chaos in which the surface was shaken laterally [13]. This is the basis of the physical model and experiment to be described next.

The main goal of this study is: can we estimate the locations of unstable equilibria (saddle-points) based on limited information associated with transient trajectories, especially based on necessarily noisy experimental data. A number of alternative system identification techniques that rely on processing time series have been developed for various applications [14]. Restoring force surface (RFS) analysis [15,16], nonlinear autoregressive moving average with exogenous inputs (NARMAX) modeling [17–20], and Hilbert transform-based data decomposition [21,22] have all been proved to be effective methods to explore the nonlinear behavior of a system using experimental data. In this study, we specifically focus on identifying unstable equilibrium points from experimental data along with the local dynamics. The specific system chosen has the advantage that it can be modeled unambiguously, and hence provide simulated data for comparative purposes. It is also relatively easy to conduct experiments on, especially with the ability to machine a surface shape to high accuracy, and measure motion using relatively high-speed digital cameras.

### 1.1. The physical model

Motivated by the aforementioned example of the snap-through buckling of a shallow elastic arch [12], consider the 2D surface as shown in Fig. 1.

This surface has five equilibrium points. Two minima  $W1 : (x = -89.01, y = 5.67)$  and  $W2 : (x = 93.82, y = 4.34)$ ; two saddle points  $S1 : (x = -12.86, y = 75.66)$  and  $S2 : (x = -11.27, y = -72.68)$ ; and a maximum (hill-top)  $H : (x = -4.74, y = -3.19)$  which is close to the origin (the unit is mm). In terms of the arch analogy, we can associate  $x$  with a vertical deflection, and  $y$  with an angle, so that the two minima represent the initial and snapped-through (stable) equilibria; and the two saddles represent predominantly angled configurations that the system will typically pass through. However, although the motivation derives from a continuous elastic system, we can study this shape directly, by placing a relatively small ball on the surface, and allowing it to respond dynamically under gravity. For a physically reasonable scale we choose to describe the surface (in terms of mm) using,

$$Z(x, y) = 8.333 - 0.04733x - 0.01737y + (-5012.18x^2 + 0.2984x^4 - 2739.2y^2 + 0.2415y^4 + 0.5369x^2y^2) \times 10^{-6}, \tag{1}$$

shown as a contour plot in Fig. 1a, and where the stable equilibria are marked by solid circles, the saddles by crosses, and the hill-top as an open circle. We note that the system is not quite symmetric in  $x$  or  $y$ , the small bias terms reflects the non-generic nature of pure symmetry in physical systems.

With the assumption of pure rolling, i.e. no slipping or bouncing, and linear viscous damping, the equations of motion of the ball on this surface are

$$\begin{aligned} (1 + Z_x^2)\ddot{x} + Z_x Z_y \ddot{y} &= -C_1 \dot{x} - Z_x \left[ \frac{5}{7}g + Z_{xx}\dot{x}^2 + 2Z_{xy}\dot{x}\dot{y} + Z_{yy}\dot{y}^2 \right] \\ Z_x Z_y \ddot{x} + (1 + Z_y^2)\ddot{y} &= -C_2 \dot{y} - Z_y \left[ \frac{5}{7}g + Z_{xx}\dot{x}^2 + 2Z_{xy}\dot{x}\dot{y} + Z_{yy}\dot{y}^2 \right] \end{aligned} \tag{2}$$

where  $Z(x, y)$  is defined in Eq. (1), the subscripts represent partial derivatives,  $g$  is the gravitational acceleration,  $C_1$  and  $C_2$  are damping ratios. In this physical model, the damping ratios in  $x$  and  $y$  direction can be assumed to be equal, i.e.,  $C_1 = C_2$  and

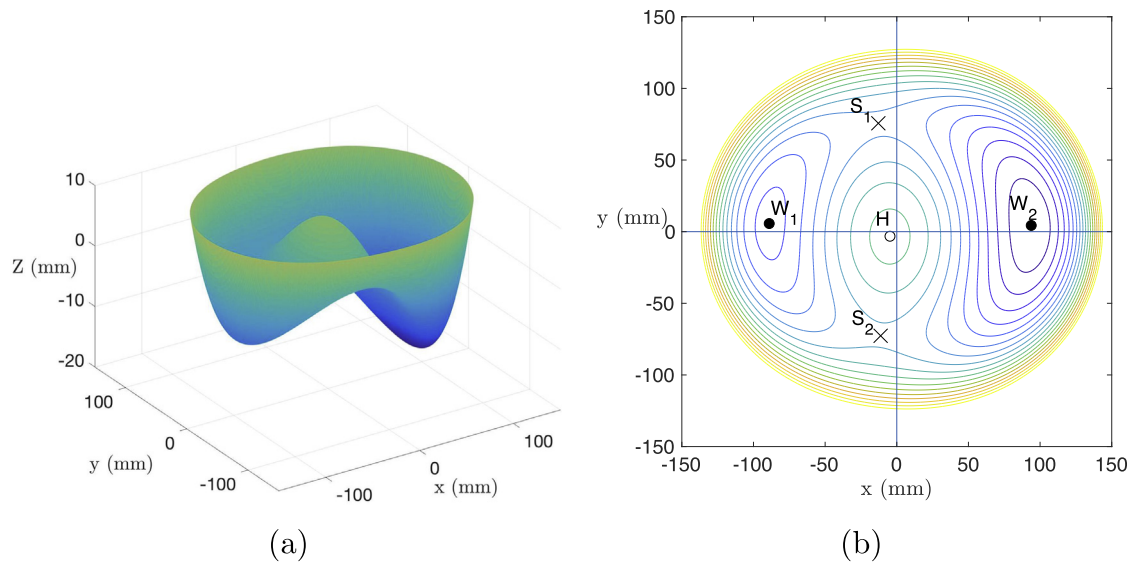


**Fig. 1.** (a) The shape of potential energy surface; the Z-direction has been elongated to exhibit the features of the surface. (b) Contour plot of the surface, the crosses are saddle points, solid circles are stable equilibria and hollow circle is the unstable equilibrium.

will be relatively small. In the simulation, the magnitude of the damping coefficient is 0.4 (1/s); this value is determined by the logarithmic decrement of experimental free-decay data [13]. It is noted that since the surface is globally bounded, the ball will not roll off to infinity. Furthermore, some of the terms appearing in Eq. (2) can be neglected if the surface is relatively shallow, although no such approximation is included in this work.

## 2. Experiment

### 2.1. Experimental setup

To produce this surface, a piece of black Delrin plastic block was chosen to route the surface from Eq. (1). And coupled with a small (21.95 mm diameter) rubber-coated steel ball, the Delrin surface could provide sufficient friction to guarantee rolling motion of the ball (see Fig. 2a). The motion of the ball was then tracked (from above) using a relatively high-speed digital camera (the black surface color helped to provide contrast with the (light-colored) ball). The surface was produced using a CNC milling machine by exactly matching the shape described by Eq. (1) to very high resolution (0.003 mm). Fig. 2b shows the experiment setup. A high-speed camera (Basler acA640–750uc with AZURE-0412ZM) was located approximately 700 mm above the surface to capture the motion of the geometric center of the ball in terms of instantaneous pixel locations (resolution 1 pixel = 0.625 mm, frame rate = 198 Hz). The videos were processed in MATLAB to extract the position of the ball's center at each frame.

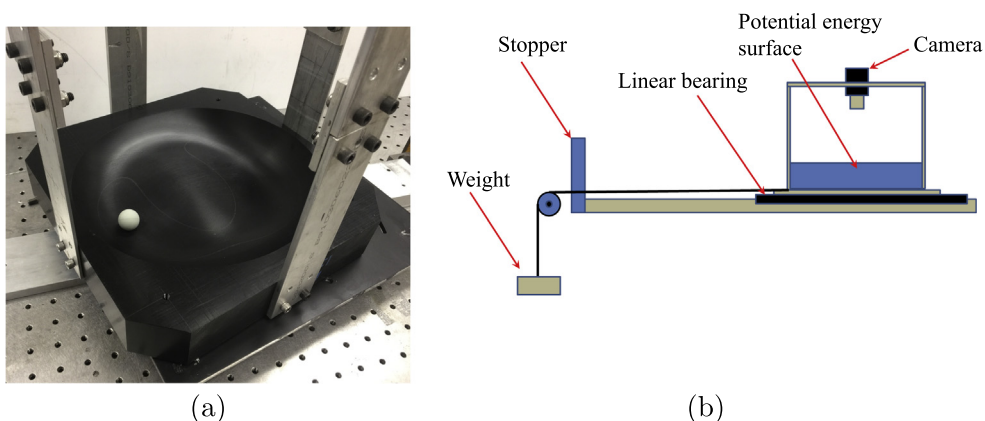


**Fig. 2.** (a) The Delrin surface used in experiment; (b) Schematic of experimental setup.

A key component in the approach described in this paper centers on energy. Despite a small amount of damping, we are essentially dealing with a conservative system, such that the initial conditions used to generate trajectories set the total energy of a given trajectory. Since the aim of this paper is to assess the extent to which trajectories are influenced by saddle-points it is necessary to encourage trajectories to at least pass relatively close to a saddle. Theoretically, and given the small amount of damping present, it is possible to choose an exact set of initial conditions such that the ensuing trajectory will come to rest exactly on the saddle. In practice this is not possible of course; we wish to generate transients that come into the vicinity of a saddle's location and at relatively low speed, and thus initial conditions need to be carefully controlled. Although this is not an issue in numerical simulations, in an experimental context this requires some effort. Two types of initial condition were used in the experiment. The first type is to release the ball at different locations (and thus potential energy) on the surface with zero initial velocity. The second type is to start the ball at rest at one of the stable equilibrium and provide the ball a certain initial velocity (kinetic energy) in specific directions. The first approach was relatively easy to achieve. In order to facilitate the second type of initial condition, a release system was designed which is shown schematically in Fig. 2b.

The nonlinear surface was attached directly onto a linear bearing, the moving part of which was connected to a weight. After the weight was released, it would pull the bearing along with the surface and camera to move under constant acceleration, until the bearing hit the stopper. The advantage of a constant acceleration is that it enabled the rubber-coated ball to stay at the stable point until the bearing hit the stopper, at which point the motion of the ball was initiated with a somewhat prescribed initial velocity. Some refinements (based on trial and error) were incorporated, including using a cushioned material attached to the stopper to absorb energy at contact and a pair of strong magnets to prevent the surface from bouncing back after the contact. The setup used in the experiment is shown in Fig. 3a. By changing the number of weights or the releasing location, the magnitude of initial velocity could be prescribed.

In addition, the angle between the surface and the linear bearing is adjustable using the slot shown in Fig. 3b. The camera was fixed with the surface; hence, no further coordinate transformation is required. Then, by adjusting the amount of weight and the angle of the surface, the desired initial velocity could be achieved. When the ball was released with zero initial velocity, the linear bearing was fixed on the supporting table by a magnet to prevent the movement of the surface. Thus, the initial position  $(x(0), y(0))$  or the initial velocity  $(\dot{x}(0), \dot{y}(0))$  were judiciously controlled such that trajectories were generated that had a tendency to approach the suspected location of the saddle points at relatively low speeds.

An example trajectory from the experiment and from simulation (based on Eq. (2)) are shown in Fig. 4. The eigenvectors of the Hessian matrix of Eq. (1) at the saddle point are also presented as lines with arrows while the direction of the arrows indicate the stability of the eigenvectors. As the trajectories are approaching the saddle point, the velocity slows down in the hyperbolic direction while beginning to oscillate in the oscillatory direction. After the trajectories pass the saddle point, they speed up and escape in the unstable direction.

## 2.2. Experimental method

In the experiment, the frame rate of the camera was set at 198 frames per second. The videos were processed in MATLAB after collection. The original videos were converted to binary videos in which the ball is white against a black background. The location of the ball was approximated by the geometric center of the white area. In the central area of the visual field, distortion was not significant.

After the position information was extracted, the velocities and accelerations were calculated through numerical differentiation. In experimental context, noise is almost inevitable. And also, as is well known, the process of differentiation has

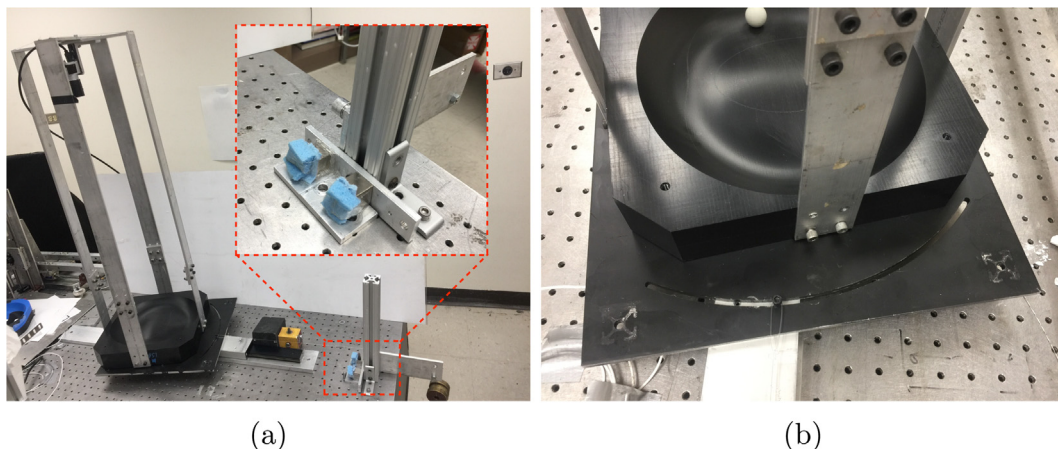
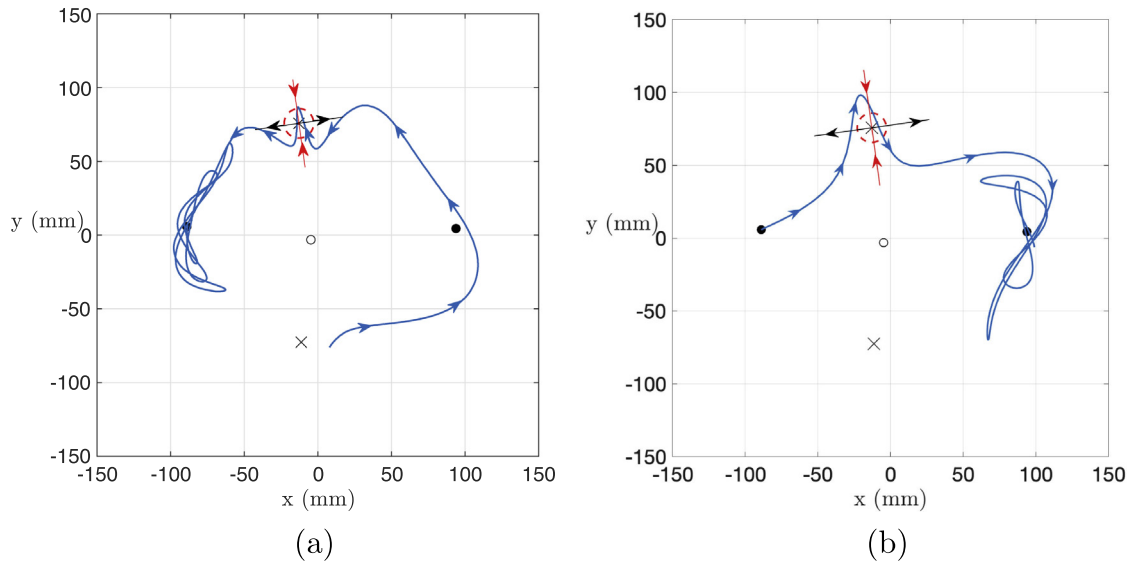


Fig. 3. (a) The experiment setup; (b) the slot for angle adjustment.



**Fig. 4.** (a) An example trajectory from experiment;  $\dot{x}(0) = 0, \dot{y}(0) = 0$ ; (b) an example trajectory from simulation,  $\dot{x}(0) \neq 0, \dot{y}(0) \neq 0$ . The diameter of the red dashed circle is 10 mm. The eigenvectors of the Hessian matrix of Eq. (1) at the upper saddle equilibrium are shown as lines with arrows; the black line represents the hyperbolic direction, the red line represents the oscillatory direction.

the tendency to amplify noise [23], and this can be seen in Fig. 5. Fig. 5 presents the position, velocity and acceleration in the x direction of one example trajectory in which the black solid lines are the noisy data of position, velocity and acceleration respectively, based on a sample trajectory from the experiment. The progressive amplification effect through numerical differentiation, especially for acceleration, can be observed clearly. To reduce the noise level, a zero-phase digital filter is used. We used the *filtfilt* method in MATLAB to reduce the noise in the position signals first and then achieve the velocities and accelerations through numerical differentiation. In Fig. 5, the red dashed line represents the filtered data.

### 3. Method to locate the saddle equilibria in the system

In this study, a local linear regression method was used to find the location of the saddle equilibria. This method requires a rough initial guess of the location of the equilibrium position being sought. In practical cases and certainly in the 2-D system here, the approximate location of the equilibrium can quite easily be estimated. For example, the estimated location of the saddle points on the surface in Fig. 2a can be simply measured by ruler.

In a more general context, consider a nonlinear dynamic system of the form:

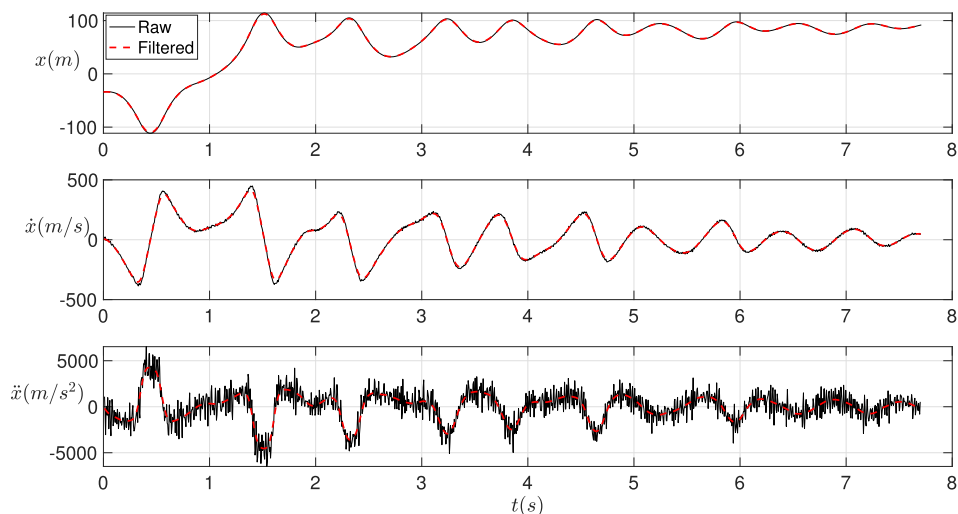


**Fig. 5.** Comparison of noisy data with filtered data from experiment.

$$\dot{\mathbf{x}} = f(\mathbf{x}), \quad \mathbf{x} \in \mathbb{R}^{2n} \tag{3}$$

where  $\mathbf{x}$  is a vector that represents the state of the system in phase space. In a  $n = 2$  DOF system,

$$\mathbf{x} = \begin{bmatrix} x \\ \dot{x} \\ y \\ \dot{y} \end{bmatrix} \tag{4}$$

Assuming  $\mathbf{x}_e$  is the vector that represents any equilibrium in the system, i.e.  $\mathbf{x}_e = [x_e; 0; y_e; 0]$ , where  $(x_e, y_e)$  is the location of the equilibrium. A new vector  $\bar{\mathbf{x}}$  is defined as  $\bar{\mathbf{x}} = \mathbf{x} - \mathbf{x}_e$ , the error in estimating the location of saddle equilibrium point. Then, Eq. (3) can be expanded around  $\mathbf{x}_e$  into a Taylor’s series as a function of  $\bar{\mathbf{x}}$ :

$$\dot{\bar{\mathbf{x}}} = f(\mathbf{x}_e) + \nabla \cdot f(\mathbf{x}_e)\bar{\mathbf{x}} + H.O.T. \tag{5}$$

The contributions from higher order terms (*H.O.T.*) are negligible in the local region of the equilibrium, i.e., we have linearized around the equilibrium. Furthermore, the constant (first) term on the right-hand side is zero at equilibrium, by definition. Thus, finding the vector  $\mathbf{x}_e$  that leads the first term to be zero, the equilibrium is located.

After we collect the dynamic information  $\dot{\mathbf{x}}$  and  $\mathbf{x}$  in the vicinity of the equilibrium, we use linear regression to build the relationship between  $\dot{\mathbf{x}}$  and  $\mathbf{x}$ , which would give us:

$$\dot{\mathbf{x}} = \mathbf{b}_{2n \times 1} + \mathbf{A}_{2n \times 2n}\mathbf{x} \tag{6}$$

where the vector  $\mathbf{b}$  is associated with the constant terms in the linear regression, and  $n$  is the degrees of freedom in the system. Then, we introduce the vector  $\bar{\mathbf{x}}$  as  $\bar{\mathbf{x}} = \mathbf{x} - \mathbf{x}_e$  into Eq. (6):

$$\dot{\bar{\mathbf{x}}} = \mathbf{b}_{2n \times 1} + \mathbf{A}_{2n \times 2n}(\bar{\mathbf{x}} + \mathbf{x}_e) = (\mathbf{b}_{2n \times 1} + \mathbf{A}_{2n \times 2n}\mathbf{x}_e) + \mathbf{A}_{2n \times 2n}\bar{\mathbf{x}} \tag{7}$$

As  $\mathbf{x}_e$  is a constant vector, of only  $n$  parameters, it would only shift the constant term in the regression model while keeping the matrix  $\mathbf{A}$  unchanged. In Eq. (7), the first and second terms on the right-hand-side are associated with the first and second terms in the right-hand-side of Eq. (5), respectively. Then, the location of equilibrium in the phase space which is represented by  $\mathbf{x}_e$  can be calculated by solving for the vector  $\mathbf{x}_e$  that satisfies the equation:

$$\mathbf{b}_{2n \times 1} + \mathbf{A}_{2n \times 2n}\mathbf{x}_e = \mathbf{0} \tag{8}$$

And the eigenvalues of matrix  $\mathbf{A}_{2n \times 2n}$  provide the linearized dynamics information near the equilibrium point  $\mathbf{x}_e$ .

#### 4. Simulation results

First, the approach was tested using the outcome of numerical simulation of Eq. (2). The study was conducted for all stable equilibria and saddle points, even though the stable equilibria were readily identified from the final locations of all trajectories. The results present similar trends for all equilibria, however in this section we specifically focus attention on the results regarding the saddle  $S_1 : (x_e = -12.863, y_e = 75.659)$  with the lower potential energy level, which was also the focus of [4]. It is worth pointing out that this method is not effective in locating the unstable (hill-top) equilibrium for this model because the trajectories rarely pass close-by. Hence, we did not apply this method to the hill-top equilibrium.

Firstly, an initial estimation of the saddle’s location is needed. The exact location of the saddle point is  $(-12.863, 75.659)$  (in mm). We rounded the numbers to achieve an “estimation”, which is  $(-10, 70)$ . The initial error, which is defined as the distance between the initial guess to the exact location, is about 6.342 mm. Then, 100 trajectories were generated in MATLAB based on solving Eq. (2) by *ODE45*. The data points that fall into a circular area around the initial estimation with specific diameters were included for linear regression. After that, the value of  $\mathbf{x}_e$  that would fit Eq. (8) was calculated. In this study, we define the error as the distance between the calculated and theoretical equilibrium, i.e.,  $\bar{e} = \|\mathbf{x}_e^{calc} - \mathbf{x}_e^{theo}\|_2$  where  $\mathbf{x}_e^{calc}$  and  $\mathbf{x}_e^{theo}$  are the calculated and the theoretical location of the equilibrium, respectively. This error is used as a measure of the accuracy of the method.

As discussed previously, the assumption that higher order terms are negligible would only be valid in a small region around the equilibrium. Hence, the diameter of the circular area is a parameter in this method. Fig. 6 shows the variation of error with the diameter of the circle area.

For a local vicinity characterized by a circle of diameter of 10 mm (the smallest area used in simulation), the new error is 0.855 mm (based on the first iteration) which is significantly smaller than the starting estimation. With an increase in the diameter of the area, the error is also increasing. The reason is that the nonlinearities (second- and higher-order terms) are no longer negligible as the diameter grows. Of course, if the diameter is sufficiently large that more than one equilibrium is encompassed, then the approach would not be expected to work.

To achieve more accurate results, another round of local linear regression can be executed based on the estimated location of the equilibrium from the previous calculation. The calculated equilibrium from the previous ‘round’ is the new initial estimation and the data points that fall into a circular area around this new estimation are included for subsequent linear regression. Fig. 7 presents the variation of error with the number of rounds of regression executed. As suggested by the plot,

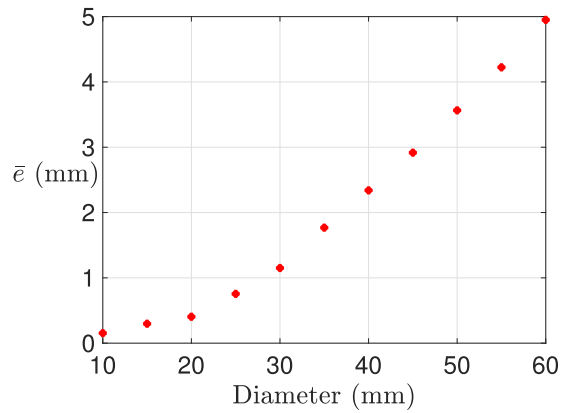


**Fig. 6.** Variation of error—the distance between calculated and theoretical equilibrium with the diameter of the circle area in simulation, where  $\bar{e} = \|\mathbf{x}_e^{calc} - \mathbf{x}_e^{theo}\|_2$ .

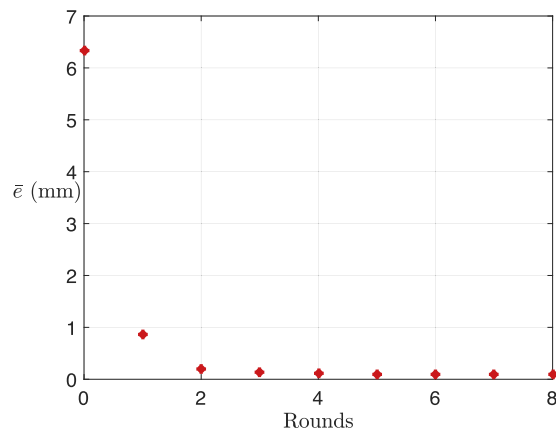


**Fig. 7.** Variation of error with rounds of regression executed in simulation. The diameter of the circular area is 10 mm.

the distance rapidly decreases and converges to 0.096 mm after only four rounds of regression. When applying this method, the validity of the result can be verified by the convergence tendency.

Along with the location of the equilibrium, this method can also provide linearized dynamics around the equilibrium, like the stability of the equilibrium, natural frequencies and damping ratio. For a saddle-point equilibrium, the frequency along the stable manifold is difficult to measure directly in an experiment. In Eq. (5),  $\nabla \cdot f(\mathbf{x}_e)$  is the linearized Jacobian matrix around the equilibrium. Thus, by finding the eigenvalues of  $\nabla \cdot f(\mathbf{x}_e)$ , the stability of equilibrium and the frequencies on the stable manifold that relates to the transient oscillatory motion near the saddle point can be determined.

Table 1 lists the eigenvalues at the saddle points along with the eigenvalues calculated by linear regression with different diameters in the fourth round. In the predominantly hyperbolic direction, which is unstable/stable, a pair of real eigenvalues exist, while in the oscillatory direction we obtain a pair of complex conjugate eigenvalues. The first row are the eigenvalues from theory. The eigenvalues from different local areas suggests that the accuracy of the eigenvalues is compromised with the increase of the area's diameter, as expected. Table 2 illustrates the variation of eigenvalues from different rounds of regression. The convergence tendency can also be observed in the eigenvalues. After the fourth round, the variation of eigenvalues between different rounds are trivial.

## 5. Experimental results

Using experimental data, a total number of 105 valid trajectories were collected. A valid trajectory is defined as the one in which the shortest distance between the trajectory to the equilibrium to be studied is smaller than 5 mm, i.e., the trajectory must pass into a circular area with diameter of 10 mm around the estimated location of the saddle point. The same initial estimated location (6.342 mm away from the exact location of the equilibrium) is used for the first round of regression. Similar to the simulation results, multiple rounds of regression were conducted and the influence of the area's size was again assessed.

**Table 1**  
Comparison of calculated eigenvalues with different diameters in the fourth round in simulation.

	Hyperbolic direction		Oscillatory direction	
	Positive	Negative	Real	Imaginary
Theory	4.621	-5.421	-0.400	8.996
Diameter(mm)				
10	4.616	-5.480	-0.408	8.922
20	4.659	-5.255	-0.477	8.975
40	4.638	-5.483	-0.495	9.233
80	5.176	-6.651	-0.652	8.677

**Table 2**  
Eigenvalues in theory compared with eigenvalues calculated from linear regression from different rounds in simulation, for a circular area of 10 mm diameter.

	Hyperbolic direction		Oscillatory direction	
	Positive	Negative	Real	Imaginary
Theory	4.621	-5.421	-0.4	8.996
Round				
1	5.261	-6.069	-0.401	7.876
2	4.503	-5.567	-0.407	9.106
3	4.633	-5.483	-0.408	8.920
4	4.616	-5.480	-0.409	8.922
5	4.613	-5.480	-0.409	8.926
6	4.609	-5.491	-0.410	8.934
7	4.609	-5.491	-0.410	8.934
8	4.609	-5.491	-0.410	8.934

Fig. 8 presents the sensitivity of the error with rounds of regression. Fig. 8a shows that the distance reduces to 1.362 mm in the first round of regression. After the fourth round of regression, the error converges to 0.787 mm which is 87.59% smaller than the initial error of 6.342 mm. Table 3 presents the eigenvalues from difference rounds. In Fig. 8b, the variable  $\Delta \bar{e}$  is defined as  $\Delta \bar{e} = \bar{e} - \bar{e}|_{Round \rightarrow \infty}$  to compare the convergence of the experimental result with the simulation result, because error in the simulation result is smaller than the experiment result. The experimental results exhibit similar convergent tendency.

Fig. 9 compares the relative experimental and simulation errors with respect to different diameter of the circular area. It can be seen that the experimental result exhibits a similar trend to the simulation result. For both experimental and simulation results, the errors increase with the diameter in a relative slow rate when the diameter is not greater than 20 mm. When the diameter is larger than 25 mm,  $\Delta \bar{e}$  increases with the diameter more rapidly and a linear relationship between  $\Delta \bar{e}$  and the diameter is exhibited in Fig. 9. The eigenvalues from Table 4 illustrate the variation of eigenvalues with the diameter of the area. Comparing with the converged eigenvalues after six rounds of regression, the accuracy of the eigenvalues is comparatively good before the diameter increases to 80 mm. This tendency is the same as in the simulation results.

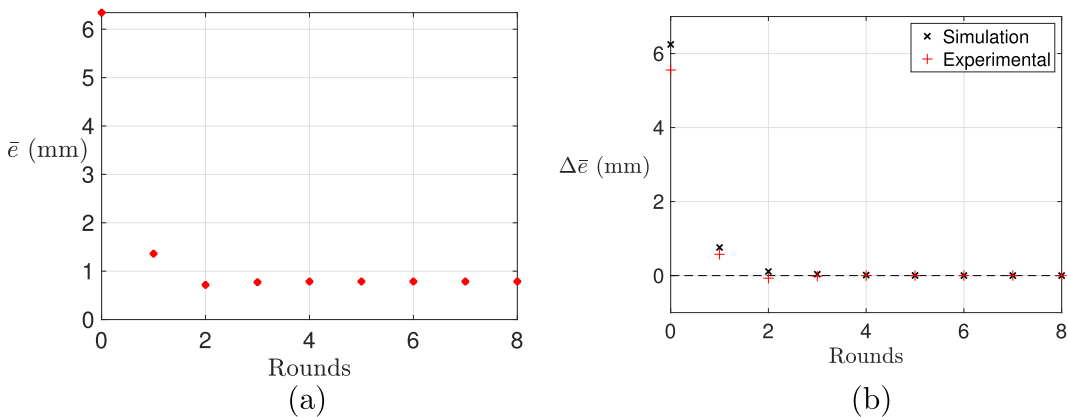


**Fig. 8.** Variation of error with the rounds of regression executed for a circular area of 10 mm diameter. (a) The result from experiment; (b) comparison of experiment and simulation result ( $\bar{e}$  in Fig. 7), where  $\Delta \bar{e} = \bar{e} - \bar{e}|_{Round \rightarrow \infty}$ ,  $\bar{e} = \|\mathbf{x}_e^{calc} - \mathbf{x}_e^{theo}\|_2$ .

**Table 3**

Eigenvalues calculated from linear regression in different round in experiment for a circular area of 10 mm diameter.

Round	Hyperbolic direction		Oscillatory direction	
	Positive	Negative	Real	Imaginary
1	5.350	-5.756	-0.113	8.960
2	4.419	-4.856	-0.120	10.319
3	4.500	-4.902	-0.097	10.212
4	4.513	-4.915	-0.099	10.214
5	4.517	-4.922	-0.099	10.207
6	4.517	-4.922	-0.099	10.207
7	4.517	-4.922	-0.099	10.207
8	4.517	-4.922	-0.099	10.207

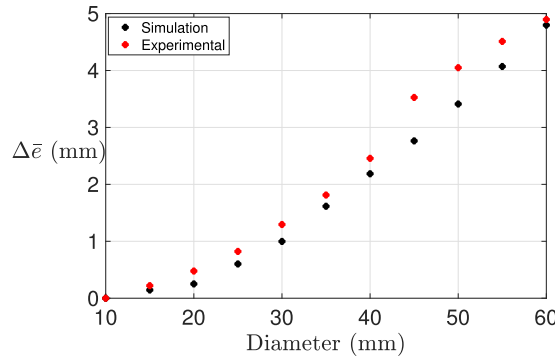


**Fig. 9.** Comparison of the relative errors of experimental and simulation result in with respect to different diameter of the circular area.  $\Delta\bar{e} = \bar{e} - \bar{e}|_{d=10}$ , where  $\bar{e} = \|\mathbf{x}_e^{calc} - \mathbf{x}_e^{theo}\|_2$  and x-axis represents the diameter of the circular region.

**Table 4**

The converged eigenvalues in theory compared with eigenvalues calculated from linear regression with different area size in the fourth round in experiment.

	Hyperbolic direction		Oscillatory direction	
	Positive	Negative	Real	Imaginary
Converged	4.517	-4.922	-0.099	10.207
Diameter(mm)				
10	4.513	-4.915	-0.099	10.214
20	4.637	-5.127	-0.163	10.187
40	4.381	-4.979	-0.193	10.157
80	4.397	-4.332	-0.293	9.316
120	4.154	-4.4629	-0.367	8.209

5.1. The influence of available trajectories

As presented previously, a good estimation can be calculated from all 105 available trajectories collected in the experiment. However, another important question to be answered is how many trajectories or data points would lead to a “good enough” result. Even though the more important factor would be the number of data points, in experiments, the data is collected in the form of trajectories. Hence, we chose the number of trajectories as the variable to be studied.

We randomly chose a certain number of trajectories from the library of the total 105 available trajectories, and used our method to find the location of the equilibrium based on this subset. This process is repeated 100 times. For each run, error, that is  $\bar{e}$  which is defined as  $\bar{e} = \|\mathbf{x}_e^{calc} - \mathbf{x}_e^{theo}\|_2$ , was recorded. In addition, the number of data points that fall into the circle area with 10 mm diameter around the estimated location of the saddle point was also collected. Then, the means and standard deviations of  $\bar{e}$  and the average data points were calculated. Fig. 10 presents the variation of means and standard deviation of  $\bar{e}$  and the averages of available data points with the number of trajectories.

When there are only 10 trajectories, both the means and standard deviations of  $\bar{e}$  are relatively large. As the number of available trajectories increases to 20, the mean and standard deviation reduce significantly. Further increasing the amount of trajectories, the mean of  $\bar{e}$  only changes moderately, but the standard deviation keeps decreasing. Part of this decline is due to the fact that there are only 105 available trajectories in total; as the amount of trajectories gets closer to 105, the standard deviation would definitely reduce. However, the decreases in mean and standard deviation from 10 to 20 trajectories

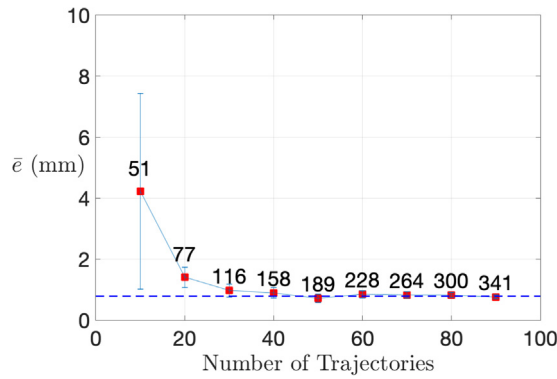


**Fig. 10.** Variation of means and standard deviations of  $\bar{e}$  with the number of trajectories. The red dots are the means of  $\bar{e}$  while the error bars show 1/4 of the standard deviation. The numbers next to the red dots are the average number of data points that fall into a circular area with 10 mm diameter around the equilibrium. The black dashed line represents the value of  $\bar{e}$  achieved by all 105 available trajectories from experiment, where  $\bar{e} = \|\mathbf{x}_e^{calc} - \mathbf{x}_e^{theo}\|_2$ .

suggests that a threshold exists. When the amount of trajectories is low, the random measurement error can dominate the data and compromises the accuracy. As the number of trajectories increase, the actual behavior of the dynamic system dominates and the accuracy of the calculated equilibrium increases.

5.2. Robustness against noise

In Fig. 5, it shows that with a properly tuned filter, the noise can be reduced effectively in the experiment. The total variation method [24,25] has also been proven to be an effective technique for extracting information from noisy data. In the experiment, the magnitude of the noise level is difficult to control. Hence, the influence of noise is studied through simulations. The noise is introduced into the simulated position data and amplified through numerical differentiation to replicate what happens in a real, noisy experiment. The new position vector  $\mathbf{R}$  is defined as:

$$\mathbf{R} = \mathbf{r} + \eta\mathbf{Z} \tag{9}$$

where  $\mathbf{r}$  is the original position vector from simulation without noise;  $\mathbf{Z}$  is a vector of independent identically distributed Gaussian entries with zero mean and unit standard deviation and  $\eta$  is the magnitude of noise. After the noise is added, to simulate the scenario in the experiment, we use numerical differentiation to calculate the velocities and accelerations. One could expect the noise would be amplified significantly through numerical differentiation. In Fig. 11, the accelerations of an example trajectory are presented. The blue lines are the original data without noise, the red lines are the data with noise achieved from numerically differentiating the position data  $\mathbf{R}$  with respect to time twice.

In the simulation, we first collect 100 trajectories that pass the vicinity of the equilibrium point by using ODE45 in MATLAB to solve Eqns. (2) numerically and add the noise as described above to the trajectories. In the ODE45 solver, the sampling rate is specified to be the same as the experiment (198 samples per second), hence, the same filter that is used previ-

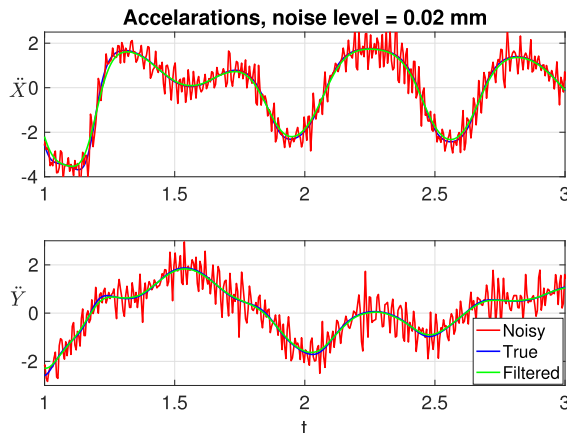


**Fig. 11.** Comparison of the actual accelerations, accelerations with noise and the noised data after the low-pass filter in simulation.

**Table 5**

Comparison of error, i.e.,  $\bar{e} = \|\mathbf{x}_e^{calc} - \mathbf{x}_e^{theo}\|_2$ , under different levels of noise, with and without filtering. The frequencies solved from the governing equation for the hyperbolic and oscillatory directions are N/A and 1.4318, respectively.

Noise level $\eta$ (mm)	Noisy			Filtered		
	Error $\bar{e}$ (mm)	Frequencies (Hz)		Error $\bar{e}$ (mm)	Frequencies (Hz)	
0	0.562	N/A	1.426	0.980	N/A	1.443
0.01	0.930	N/A	1.501	0.920	N/A	1.445
0.02	7.280	N/A	1.555	0.616	N/A	1.444
0.03	5.264	N/A	1.391	0.880	N/A	1.443
0.04	5.575	N/A	1.486	0.583	N/A	1.445

ously for experimental data can be used for simulation data. Then, we applied our method twice on the data: one on the noisy data, while the other one on the filtered data—similar to the experiment, we applied the *filtfilt* method on the position signal and then used numerical differentiation to get the velocities and accelerations. In Fig. 11, the accelerations are presented. The filtered data are represented by the green lines while the red lines are noisy data. One can see that the filtered data can basically capture the behavior of the original data correctly as the green lines are close to the blue lines which represent the actual accelerations achieved from the *ODE45* solver.

In Table 5, the impact of the noise level is shown. The N/A under the frequencies column indicates that the system is hyperbolic (not oscillatory) in the associated direction. In general, for both raw data and filtered data, the distance between the calculated and theoretical equilibrium increases with the increase of noise level. For a small noise level, like  $\eta = 0.01$  mm, good estimations can be achieved from both the noisy data and filtered data. However, as the noise level increases further, the result from the filtered data is significantly better than the results from noisy data. By comparing the error from noisy data and distance from the filtered data, one can find that the result from filtered data are comparatively more robust against an increase of noise level. And both errors and frequencies are robust against the increase of noise level.

Hence, this method can provide robust inference with small noise level without any noise reduction technique. However, for larger noise levels, it would be better to preprocess the data to reduce the noise first.

## 6. Conclusions

In this study, a method to locate saddle-point equilibria in nonlinear dynamic systems is proposed and tested by both simulation and experiment. The simulation and experimental results exhibit similar tendencies. This method estimates the location of stable or saddle equilibria in this dynamical system effectively. In both experiment and simulation, after certain rounds of regression, a relatively precise estimation of the equilibrium's location was achieved. In experiments, the typical error of the estimated equilibrium location is less than 0.79 mm. Comparing to the global system which is 300 mm  $\times$  300 mm, the relative error is only on the order of 2.6%. At the same time, the eigenvalues around the equilibrium can also be estimated.

In this study, the damping is assumed to be linear viscous damping—as the name suggests—which is linear in the governing equations of motion, and the coefficients associated with the nonlinear velocity terms are small around the equilibrium. Hence, the majority of the nonlinearities are associated with position. For a system with nonlinear damping, it would make sense to consider the system as a four dimensional system and conditions on velocities should also be applied when collecting the portions of trajectories for regression. In addition, the local neighborhood around an equilibrium in this study is defined as the area of a circle. In some other systems, a distorted shape defined by the local eigenvectors might lead to a better balance between the size of the area and the amount of available data points. In theory, one could tune the method by successively changing the size and shape of the local neighborhood as the eigenvalues get computed during successive rounds. It is the authors goal to apply this approach to systems of higher-order.

## Acknowledgement

This work was supported by the National Science Foundation under award numbers 1537349 and 1537425.

## References

- [1] R.H. Lyon, *Statistical Energy Analysis of Dynamical Systems: Theory and Applications*. MIT press, Cambridge, 1975.
- [2] L.N. Virgin, *Introduction to Experimental Nonlinear Dynamics: A Case Study in Mechanical Vibration*, Cambridge University Press, 2000.
- [3] J. Guckenheimer, P. Holmes, *Nonlinear Oscillations, Dynamical Systems, and Bifurcations of Vector Fields*, vol. 42, Springer Science & Business Media, 2013.
- [4] J. Zhong, L.N. Virgin, S.D. Ross, A tube dynamics perspective governing stability transitions: an example based on snap-through buckling, *Int. J. Mech. Sci.* 149 (2018) 413–428.
- [5] J.M.T. Thompson, H.B. Stewart, *Nonlinear Dynamics and Chaos*, John Wiley & Sons, 2002.
- [6] S.D. Ross, A.E. BozorgMagham, S. Naik, L.N. Virgin, Experimental validation of phase space conduits of transition between potential wells, *Phys. Rev. E* 98 (5) (2018) 052214.
- [7] L.E. Payne, D.H. Sattinger, Saddle points and instability of nonlinear hyperbolic equations, *Israel J. Math.* 22 (3–4) (1975) 273–303.

- [8] F.J. Flanigan, J.L. Kazdan, *Calculus Two: Linear and Nonlinear Functions*, Springer Science & Business Media, 1998.
- [9] M. Benzi, G.H. Golub, J. Liesen, Numerical solution of saddle point problems, *Acta Numerica* 14 (2005) 1–137.
- [10] R. Glowinski, J.T. Oden, Numerical methods for nonlinear variational problems, *J. Appl. Mech.* 52 (1985) 739.
- [11] A. Battersmann, E.W. Sachs, Block preconditioners for kkt systems in pde-governed optimal control problems, *Fast solution of discretized optimization problems*, Springer, 2001, pp. 1–18.
- [12] R. Wiebe, L.N. Virgin, On the experimental identification of unstable static equilibria, *Proc. R. Soc. London A* 472 (2190) (2016).
- [13] L.N. Virgin, T.C. Lyman, R.B. Davis, Nonlinear dynamics of a ball rolling on a surface, *Am. J. Phys.* 78 (2010) 250–257.
- [14] J.P. Noël, G. Kerschen, Nonlinear system identification in structural dynamics: 10 more years of progress, *Mech. Syst. Signal Process.* 83 (2017) 2–35.
- [15] S.F. Masri, T.K. Caughey, A nonparametric identification technique for nonlinear dynamic problems, *J. Appl. Mech.* 46 (2) (1979) 433–447.
- [16] P. Saad, A. Al Majid, F. Thouverez, R. Dufour, Equivalent rheological and restoring force models for predicting the harmonic response of elastomer specimens, *J. Sound Vib.* 290 (3–5) (2006) 619–639.
- [17] Q. Chen, K. Worden, P. Peng, A.Y.T. Leung, Genetic algorithm with an improved fitness function for (n) arx modelling, *Mech. Syst. Signal Process.* 21 (2) (2007) 994–1007.
- [18] Z.K. Peng, Z.Q. Lang, C. Wolters, S.A. Billings, K. Worden, Feasibility study of structural damage detection using narmax modelling and nonlinear output frequency response function based analysis, *Mech. Syst. Signal Process.* 25 (3) (2011) 1045–1061.
- [19] K. Worden, R.J. Barthorpe, Identification of hysteretic systems using narx models, part i: evolutionary identification, *Topics in Model Validation and Uncertainty Quantification*, vol. 4, Springer, 2012, pp. 49–56.
- [20] K. Worden, R.J. Barthorpe, J.J. Hensman, Identification of hysteretic systems using narx models, part ii: a bayesian approach, *Topics in Model Validation and Uncertainty Quantification*, vol. 4, Springer, 2012, pp. 57–65.
- [21] M. Feldman, Time-varying vibration decomposition and analysis based on the hilbert transform, *J. Sound Vib.* 295 (3–5) (2006) 518–530.
- [22] M. Feldman, Considering high harmonics for identification of non-linear systems by hilbert transform, *Mech. Syst. Signal Process.* 21 (2) (2007) 943–958.
- [23] F.B. Hildebrand, *Introduction to Numerical Analysis*, Courier Corporation, 1987.
- [24] S.L. Brunton, J.L. Proctor, J.N. Kutz, Discovering governing equations from data by sparse identification of nonlinear dynamical systems, *Proc. Nat. Acad. Sci.* 113 (15) (2016) 3932–3937.
- [25] L.I. Rudin, S. Osher, E. Fatemi, Nonlinear total variation based noise removal algorithms, *Physica D* 60 (1–4) (1992) 259–268.